Projections of Southern Hemisphere Tropical Cyclone Track Density using CMIP5 models

Submitted to Climate Dynamics in June 2018

Samuel S. Bell[1],

Savin S. Chand[1],

Kevin J. Tory[2],

Andrew J. Dowdy[2],

Christopher Turville[1] and

Harvey Ye[2]

Corresponding Author: Samuel S. Bell,

E-mail: ss.bell@federation.edu.au

Phone: 04 599 290 71

[1] Centre for Informatics and Applied Optimization, Federation University Australia, Ballarat 3357, Australia

[2] Research and Development Branch, Bureau of Meteorology, Melbourne 3001, Australia

Abstract

A recently validated algorithm for detecting and tracking tropical cyclones (TCs) in coarse resolution climate models was applied to a selected group of 12 models from the Coupled Model Intercomparison Project (CMIP5) to assess potential changes in TC track characteristics in the Southern Hemisphere (SH) due to greenhouse warming. Current-climate simulations over the period 1970 – 2000 are first evaluated against observations using measures of TC genesis location and frequency, as well as track trajectory and lifetime in seven objectively defined genesis regions. The 12-model (12-M) ensemble showed substantial skill in reproducing realistic TC climatology over the evaluation period. To address potential biases associated with model interdependency, analyses were repeated with an ensemble of five independent models (5-M). Results from both the 12-M and 5-M models were very similar, instilling confidence in the models for climate projections. Projected changes in TC track density between the current- and future-climate (2070–2100) simulations under the Representatives Concentration 8.5 Pathways (RCP8.5) are also assessed. Overall, projection results showed a substantial decrease (~1–3 per decade) in track density over most parts of the SH by the end of the twenty-first century. This decrease is attributed to a significant reduction in TC numbers (~15–42%) consistent with changes in large-scale environmental parameters such as relative vorticity, environmental vertical wind shear and relative humidity. This study has important implications for regional-scale climate change and adaptation pathways for the vulnerable regions in the SH, particularly the small island countries in the Pacific.

Keywords: tropical cyclone, track, southern hemisphere, model projection, climate change

1. Introduction

The frequency of tropical cyclone (TC) impacts on coastal communities are directly determined by the annual number and mean trajectory of localized TCs. Improving clarity of the relationship between these characteristics and human-induced global warming can therefore help target future planning and preparation efforts to high-risk areas in the Southern Hemisphere (SH). Potential changes to future TC track densities will have regional-scale consequences to communities situated among the three TC basins in the SH, namely the South Indian basin (0 – 50°S; 30 – 90°E), the Australian region (0 – 50°S; 90 – 160°E) and the southwest Pacific basin (0 – 50°S; 160°E – 120°W).

Determinants of TC track density can be separated into two components: TC genesis (both location and frequency), and TC track direction. A number of previous studies undertaken on TC frequency projections in the SH (e.g., Murakami et al. 2012; Sugi and Yoshimura 2012; Tory et al. 2013c; Rathmann et al. 2014) have generally indicated a mild decrease in the hemisphere-wide numbers with reasonably high confidence. However, an exception was a downscaling effort (Emanuel, 2013) that found an increase in TC activity in the South Indian and western Australian regions. In contrast to TC frequency, there has been little consensus on TC track projections for the SH basins (Christensen et al. 2013; Walsh et al. 2016), potentially due to relatively fewer studies in these basins and a focus on the Northern Hemisphere in recent years (e.g., Camargo 2013; Colbert et al. 2015; Daloz et al. 2015; Wang and Wu 2015; Kossin et al. 2016; Nakamura et al. 2017; Park et al. 2017). This highlights the need for more robust quantitative assessments of projected changes in TC track densities for the SH basins using new and innovative approaches.

In recent years, attention has begun to shift towards TC track projections as numerous modelling and analytical techniques have been developed and refined to better evaluate the

49 complexities of TC tracks in climate models. This includes improvements in the often-used
50 climate models from the Coupled Model Intercomparison Project (such as CMIP5, Taylor et
51 al. 2012) in reproducing realistic large-scale environmental conditions that affect TC
52 formation (e.g., CCiA 2015; Moise et al. 2015; Chand et al. 2017) and advances in track
53 analysis techniques (e.g., Gaffney 2004; Nakamura et al. 2009; Nakamura et al. 2017; Shen et
54 al. 2018). There have also been substantial improvements in detection (and tracking) of TCs
55 in climate models, including the Okubo-Weiss-Zeta scheme (OWZ; Tory et al. 2013a) that
56 can circumvent detector dependence on model resolution, which is often cited as a limitation
57 of TC projection studies (e.g., Walsh et al. 2007; Horn et al. 2014; Daloz et al. 2015). The
58 primary aim of this study is to use state-of-the-art analysis techniques to determine if a
59 consensus on track density changes can be achieved for the SH using CMIP5 models under a
60 high emission scenario (RCP8.5; Section 2). The two main aspects of TC track density
61 changes (i.e. frequency and track direction) are investigated in seven separate study regions
62 that are objectively identified by a cluster analysis.

63 The TC detection and tracking scheme of Tory et al. (2013a) is applied to CMIP5
64 models after having undergone scrupulous validation in ERA-Interim data in terms of annual
65 numbers (Tory et al. 2013b) and tracks (Bell et al. 2018). The latter study provided an
66 objective definition of a "TC track" for applications in coarse resolution model data and also
67 recommended discarding short lived TCs (< 2-days) for optimal performance. Prior
68 application of the scheme in CMIP5 models (e.g., Tory et al. 2013c; Chand et al. 2017) found
69 that some models failed to realistically simulate a reasonable global climatology of TCs, thus
70 limiting the present study to only the 12 CMIP5 models that were deemed satisfactory by
71 those studies. Moreover, when interpreting results from multi-model ensembles, we also
72 acknowledge the concerns raised by Sanderson et al. (2015) that statistical interdependence
73 between CMIP5 models needs to be considered.

74 The outline of this paper is as follows. Section 2 contains the data, definitions and
75 methods used in the study. Section 3 provides assessment and validation of models and
76 climate projection results. Section 4 discusses the physical mechanisms that drive significant
77 projected changes in TC track densities. Finally, a summary, discussion of results and
78 prospects of future work are given in Section 5.

79 **2. Data, Definitions and Methods**

80 *a. Observational data*

81 The International Best Track Archive for Climate Stewardship (IBTrACS-WMO v03r08,
82 Knapp et al. 2010) data over the observationally consistent period (1989-2013) is used to
83 define the observed TC track climatology and to give a baseline of TC characteristics. For the
84 purpose of this study, an observed TC track is defined to begin at a the location the storm first
85 reaches a 10-minute sustained wind speed of 17 m s^{-1}, with storms not reaching this intensity
86 at any time of their lifetime excluded from the analysis. Tracks are terminated if a forecast
87 centre no longer tracks them (i.e. track information ceases in the database) or if they
88 encounter an objectively diagnosed subtropical jet (Tory and Dare 2015) after which the
89 storm has likely to have lost its physical TC characteristics.

90 *b. CMIP5 model data*

91 Twelve models from the Coupled Model Intercomparison Project phase 5 (CMIP5, Taylor et
92 al. 2012) are used in this study (Table 1). Note that CMIP5 experiments contain the current
93 generation of climate models that provide a wide array of platforms to test current and future
94 climate scenarios (e.g., Knutti et al. 2013). The two scenarios assessed in this work are (1) the
95 current-climate simulation over the period 1970 – 2000 for model evaluation and assessment,
96 and (2) the future-climate simulation over the period 2070 – 2100 under the Representative
97 Concentration Pathway 8.5 (RCP8.5) for projection analyses. RCP8.5 represents an 8.5 W m^{-}

98 ^{2} increase in radiative forcing values in the year 2100 as compared to the pre-industrial
99 emission levels (Riahi et al. 2011) and was chosen to best elucidate any changing TC
100 behaviour in a warmer climate.

101 *c. Multi-model ensembles and significance tests*

102 Differences between model physics parameterisations, as well as deficiencies in models'
103 ability to resolve atmospheric processes, can create potential biases in the results of
104 projection analyses. In this study, we statistically reduce some of these biases by combining
105 results of all models together to form a multi-model ensemble. In the analysis, results are
106 considered statistically robust if large proportions of models agree on the sign and magnitude
107 of the change. A statistical significance test to evaluate the robustness is determined at the
108 95% level and is based on a binomial distribution (e.g., Chand et al. 2017). Thus for a 12-
109 model ensemble, the number of models required to attain the 95% level of significance is 10.
110 However, this test assumes model independence, and based on the analysis of Knutti et al.
111 (2013) and Sanderson et al. (2015), some models may be in violation of this assumption. As a
112 result, we additionally employed a smaller set of independent models for all our analyses (see
113 Appendix A for details). This "smaller" multi-model ensemble is comprised of five models
114 and requires all models to agree on the sign of change to achieve the 95% significance.

115 *d. Detection and tracking*

116 The OWZ TC detection and tracking scheme (Tory et al. 2013a) is used in this study to detect
117 and track TCs in all models. The OWZ scheme has undergone scrupulous validation in
118 reanalysis data in terms of annual TC numbers and genesis positions (Tory et al. 2013b) and
119 more recently in terms of tracks at 12-hr intervals (Bell et al. 2018). Key details of the OWZ
120 detector and tracker are provided in Tory et al. (2013a) while a short summary of the scheme
121 is provided in the appendix of this paper for easy reference (Appendix B).

122 Crucially, the Bell et al. (2018) track validation study identified a limitation of the
123 tracking scheme, in that it detected a higher than expected frequency of short duration TC
124 tracks in ERA-Interim. This limitation also affected TC tracks in models (Fig. 1), and so
125 necessary steps are taken to minimise its impact on projection results following the analysis
126 of Bell et al. (2018), who showed that most of the short lifetime tracks (< 48-hr) in models
127 were likely to be associated with detector related errors. As such, TC tracks less than 2-days
128 in lifetime are removed from the analysis to achieve a more accurate climatology.

129 To be consistent with the definition of the observed TC tracks, the objective TC track
130 definition established in Bell et al. (2018) is also used here. This definition states that a TC
131 track detected by the OWZ scheme commences from the TC declaration location[1] and
132 terminates where a TC either dissipates or encounters an objectively diagnosed subtropical
133 jet.

134 *e. Cluster analysis*

135 The probabilistic curve-clustering technique of Gaffney (2004) is used to group TC tracks of
136 similar properties in space and time over the entire SH. TCs in certain sub-regions with more
137 erratic tracks have undergone further cluster analysis to elucidate more meaningful patterns
138 (see Section 3). Implementation of the clustering technique follows prior studies (e.g.,
139 Camargo et al. 2007; Chand and Walsh 2009) where linear regression mixtures are fitted to
140 each track with a pre-defined number of clusters, $k=7$ in this case (e.g., Ramsay et al. 2012;
141 Bell et al. 2018), to produce a zonally consistent solution for the SH basins (Fig. 2).

142

[1] The TC declaration location was found to best match the timing at which TCs in IBTrACS data first reached a 10-minute sustained wind speed of 17 m s^{-1}.

143 *f. Seven meridional-bounded regions*

144 Information provided by cluster analysis from the best track observations (Fig. 2a) are
145 represented as kernel density estimates that enclose 75% of the TC genesis positions in each
146 cluster to allow a direct comparison with the models. However, when the analysis was
147 repeated for the models[2] (Fig. 2b), a slight shift in the cluster position was found (e.g.,
148 meridional location of the Indian Ocean clusters). We note that when comparing TC number
149 results in different climate scenarios, changing orientations of corresponding clusters could
150 mask actual changes (or even produce spurious results), making comparisons difficult. This
151 issue is further exacerbated by the large geographical size of the study area under
152 consideration and the high number of clusters used.

153 Therefore, we decided to use the clustering results from the observations to define
154 geographically consistent regions for ease of comparison. That is, we use the 75% genesis
155 contour of each cluster in IBTrACS to define consistent regions for the entire experiment
156 (including models) instead of re-clustering each new set of model data. Given that clusters
157 are largely adjacent to each other across the hemisphere, simple meridional lines were used to
158 define the seven regions (R1–R7, Fig. 2). The positions of the meridional lines were carefully
159 chosen and adjusted to achieve as distinct regions as possible, including taking into
160 consideration the general track type of TCs in neighbouring clusters.

161 **3. Evaluation and Projection of TC Track Density Change**

162 *a. Regional genesis density and TC numbers*

163 Changes in TC track density are dependent on both TC numbers (also used interchangeably
164 with genesis frequency throughout the paper) and track directions. We start by evaluating the

[2] Note that biases exist in models causing TCs to be detected in the far eastern South Pacific (east of 225°E). These detections are excluded from this cluster analysis to avoid creating an additional arbitrary cluster.

165 ability of the 12 CMIP5 models (hereafter collectively referred to as the 12-M ensemble) to
166 simulate regional scale (R1–R7) TC genesis locations and frequencies in the SH.

167 It is evident from the analysis that the 12-M CMIP5 models can realistically simulate
168 spatial patterns of the observed genesis density estimates reasonably well in most regions
169 (Fig. 2). However, an exception is the eastern South Pacific region (i.e. farther east of R7)
170 where a number of TCs are detected by the models that were not present in the observations,
171 as also noted in prior studies (e.g., Tory et al. 2013; Chand et al. 2017). This could be
172 potentially due to climate model biases in simulating an overly zonal orientation of the South
173 Pacific Convergence Zone (SPCZ)[3] in the eastern Pacific (e.g., Brown et al. 2012; Grose et al.
174 2014). In addition, Tory and Ye (2018) investigated the different constraints that restrict TC
175 formation in a selection of CMIP5 models. They found these models were unable to correctly
176 simulate the cool sea-surface temperatures and associated dry middle troposphere that
177 inhibits TC formation in this region. The average annual number of TCs detected by the 12-M
178 ensemble in current-climate simulation was also found to compare well with the observed
179 climatology (Table 2). However, some slight overestimations were noted, particularly near
180 Madagascar (R1) where an additional ~2 TCs per year were detected.

181 We next turn our attention to regional projections of TC numbers between the current-
182 and future-climate simulations from the CMIP5 models (Table 2 and Fig. 3). Results indicate
183 a widespread reduction of TC detections by the late twenty-first century, particularly in the
184 South Indian basin (i.e., regions R1–R4). Here, each region experiences a statistically
185 significant reduction in mean climatological numbers (at the 95% significance level), with the
186 largest reduction (~42 %) occurring in R3 located between 85°E and 105°E. The region north

[3] The SPCZ is the dominant climatic feature in the south Pacific where tropical cyclone activities are often spawned, and any biases in the position and orientation of the SPCZ will have implications on tropical cyclones forming in the region.

187 of Australia (R5) experiences about a 15% reduction in TC numbers (though this is not
188 statistically significant), while there is no clear indication of any change off the east coast of
189 Australia (R6). Farther east into the South Pacific (R7), a statistically significant reduction in
190 TC numbers (~15 %) is also found.

191 We recognize that some models used in these analyses (12-M ensemble) are very
192 similar in physical characteristics and that model interdependence may complicate the
193 interpretation of multi-model ensemble results (Knutti et al. 2013; Sanderson et al. 2015). For
194 this reason, as well as to correct model biases in reproducing TC climatology in the SH (e.g.,
195 detections east of R7), our analyses were repeated with a 5-model (5-M) ensemble. Details on
196 the selection of these five models, based on independence (Knutti et al. 2013) and a number
197 of other criteria for statistical bias corrections, can be found in Appendix A. Overall,
198 projection results from the 5-M ensemble were very similar with the 12-M results (Table 2
199 and Fig. 3), instilling our confidence in the 12-M results.

200 *b. Regional TC tracks*

201 The second aspect of track density change analyzed is the frequency and direction of TC
202 tracks. Here we evaluate the ability of the five independent CMIP5 models (5-M ensemble)
203 to simulate these track characteristics in each region (R1–R7) of the SH. It is important to
204 emphasize that within some regions (R3–R7), there exists distinct westward and eastward
205 trajectories that are not well captured by the seven mean trajectories (as in Fig. 2). Therefore,
206 we sub-divide these regions by implementing a further cluster analysis with respect to two
207 clusters in an attempt to separate the tracks into two distinct types: eastward and westward
208 moving tracks (Figs 4–6)[4]. Regional track characteristics are then evaluated with measures of

[4] Note for Region-3 we found a manual split into "eastward" and "westward" more interpretable than those given by cluster analysis. Here, tracks were classified as either "eastward" or "westward" based on their longitude positions at two-thirds of their lifetime in relation to their genesis position. In addition, westward

209 mean track trajectory, mean TC lifetime and the number of eastward and westward moving
210 tracks.

211 The mean direction of TC tracks detected by the 5-M ensemble in current climate
212 simulations were found to compare quite well with the observed climatology (Figs 4–6).
213 However, the mean TC trajectory lengths were often slightly underestimated in models, for
214 example in R1 and R6-East, potentially due to biases in estimating endpoints of tracks both in
215 observations and models. In contrast to the latter result, the mean TC lifetimes were well
216 simulated in most regions (Table 4), and we note that underestimated TC trajectory lengths
217 were attributed to a slight underestimation of model tracks in the region poleward of 30°S
218 (not shown) rather than underestimated lifetimes. The observed ratios between westward and
219 eastward TC tracks in R3, R5, R6 and R7 were found to compare well with the current-
220 climate 5-M simulations (Table 3). However, we note an overestimation of the model
221 simulated westward tracks in R4 (where 48% tracked westward), causing a discrepancy with
222 observations (where just 18% tracked westward).

223 We next examine projected changes in the tracks between the current-climate and
224 future-climate (under RCP8.5) conditions (far right panel in Figs 4–6). For ease of
225 comparison, the 5-M ensemble mean trajectories for the current- ("black tracks") and future-
226 ("red tracks") climate simulations are plotted on the same axis (Fig. 7). Overall, some small
227 shifts in mean genesis locations (circles) are noted (e.g., poleward movement in R2, R3, R4
228 and R6-West under RCP8.5; see also Kossin et al. 2014; Moon et al. 2015). For the mean
229 trajectories, there seems to be no clear deviation between the current and future climate
230 simulations, although one exception appears to be the trajectory of R6-West. This trajectory
231 appears to shift from west-southwest in the current-climate to more southwestward in the

heading model tracks in the South Pacific (Region-7) that do not appear in the observed climatology are separated by an additional cluster (to a total of 3).

232 future-climate, potentially shifting mean TC landfall positions farther south over the eastern
233 coast of Australia (see also Fig. 5, bottom-right panel).

234 Furthermore, projected changes in TC numbers are also compared for the eastward
235 and westward trajectories defined earlier (for regions R3–R7; Table 3). The significant
236 decrease of TC numbers in the central South Indian (R3) was found to more heavily reduce
237 the eastward tracks (65%) than the westward tracks (39%). The decrease in TC numbers over
238 northern Australia (R5) was found to reduce the westward track numbers by 33%, yet the
239 number of eastward tracks was found to increase by 6% (although the change in the latter was
240 not considered statistically significant). Westward TC tracks in the Coral Sea region (R6)
241 were found to increase by 16%, with region wide numbers offset by an accompanying
242 decrease in eastward numbers (13%). Farther into the South Pacific (R7), projected decreases
243 in TC numbers were more evenly spread across the different track types (Table 3). For
244 completeness, projected changes in mean TC track lifetimes were also examined (Table 4)
245 but no major changes (> 1-day) were noted.

246 *c. Track density change*

247 The prior sections have separately given detailed analyses of the two aspects of TC track
248 density changes between the current- and future- climate model simulations. Here, we
249 combine these two aspects into a single measure called “TC activity” that can collectively
250 explain changes in TC track density under the RCP8.5 scenario. TC activity is measured by
251 accumulating the number of unique TCs either forming or entering a 2.5° x 2.5° grid box over
252 the entire SH basin for both current- and future-climate simulations using the 12-M ensemble
253 of CMIP5 models (Fig. 8). TC activity is found to decrease significantly (up to 3 TCs per
254 decade) throughout the South Indian basin extending through to 135°E (i.e. including R1–
255 R4, and R5-West) in the future-climate. The decrease in TC activity is most concentrated

centrally in the basin (R3), occurring over the open ocean. However, the coastal communities of east Africa, Madagascar and western Australian region are likely to experience a similar decrease in activity (~1–2 per decade). Overall, these decreases are likely from the significant decreases in TC numbers over those regions (Section 3a) rather than projected changes in track directions that showed little deviation (Section 3b).

East of 135°E, projected changes in TC activity are comparatively smaller in magnitude (mostly within ±1 TC per decade). Notably, the small patch of increased TC activity alongside the eastern coast of Australia is supported by significant agreement between individual models of the 12-M ensemble (not shown). TC activity here is influenced by the number and mean trajectory of TCs in the R5-East and R6-West sub-clusters. In R6-West, TC numbers were found to slightly increase in magnitude for both the 12-M and 5-M ensembles (Table 3). The mean trajectory of R6-West was also found to move more favourably into this patch of increased density (Fig. 7). However, the combination of these effects only amounts to a very small increase in the coastal TC activity (~1 per twenty years). Furthermore, it is beyond the scope of this study to attribute poleward or other shifts in track density to climate change as it may require complicated downscaling techniques (e.g., Walsh and Katzfey 2000; Emanuel 2013). East of the dateline (R7), TC activity was generally found to decrease (~1 per decade) and was attributed to decreasing TC numbers in this region as also noted in several other previous studies (e.g., Tory et al. 2013c).

4. Changes in the Large-scale Environment

As seen earlier, substantial changes in TC activity between the current-climate simulation and future-climate RCP8.5 simulation were attributed to changes in TC numbers rather than tracks. Therefore, the large-scale environmental parameters associated with TC formation are empirically analysed here to better understand these projected changes. TC formation is

280 controlled by a set of dynamic and thermodynamic environmental parameters (e.g., Gray
281 1975; Tory and Frank 2010), noting that not all of these parameters may be relevant on
282 climate time scales.

283 The dynamic parameters evaluated include relative vorticity at 850 hPa, environmental
284 vertical wind shear between 850 and 200 hPa and low-level convergence at 850 hPa. The
285 only thermodynamic parameter evaluated is mid-level relative humidity at 700 hPa. Values of
286 large-scale fields (such as *u* and *v* components of winds at respective levels) needed to
287 compute these parameters are taken during the peak of the SH TC season (i.e. December to
288 February), and then composited over all models in consideration to form multi-model
289 ensembles for the current- and future-climate simulations (Figs 9 and 10).

290 To a large extent, all large-scale environmental parameters exhibit less favourable
291 future conditions for TC development in the South Indian Ocean (west of 130°E; regions R1-
292 R4) where models project a strong reduction in climatological numbers between the current-
293 and future-climate (Fig. 3). Cyclonic relative vorticity is reduced in the main genesis zone
294 (~8 – 15°S), particularly evident in R1 around Madagascar, and appears to be the main factor
295 inhibiting TC development here in the future climate (Fig. 9a; Fig. 10a). Reduced mid-level
296 relative humidity (Fig. 9c; Fig. 10c), as well as reduced low-level convergence (Fig. 9d), are
297 also consistent with a reduction in TC numbers.

298 In R5 north of Australia (~130 – 155°E), we see a slight enhancement of cyclonic
299 vorticity (Fig. 9a; Fig. 10a), particularly near the east Australian coast (~ 140°E, 12°S). While
300 these conditions should favour development of TCs, we suspect that projected decline in the
301 number of TCs in this region is strongly modulated by substantially reduced low-level
302 convergence (Fig. 9d) and to a lesser extent by relative humidity (Fig. 10c). In the two South
303 Pacific regions (R6 and R7; 155°E – 135°W), increased environmental vertical wind shear

304 (Fig. 9b), and to a lesser extent reduced low-level relative vorticity and convergence (Fig. 9a
305 and Fig. 9d), appear to be the main factors inhibiting TC formation.

306 **5. Discussion and Summary**

307 A comprehensive study was undertaken in the SH to examine the likely projected changes in
308 TC track densities due to anthropogenic greenhouse warming. Climate model simulations
309 from the CMIP5 experiments were used to assess changes in TC track densities between the
310 current (1970–2000) and future-climates (2070–2100). Two multi-model ensembles were
311 used, a 12-M and a 5-M version, with the latter only containing models that met more strict
312 criteria such as model independence.

313 Unlike previous climate projection studies for the SH basins, we have objectively
314 created seven regions (R1–R7) based on cluster analysis where each region is
315 characteristically distinct in terms of mean genesis location and track shapes. After robust
316 statistical assessment and validation of TC numbers and tracks for each region using
317 observed records from the IBTrACS database, CMIP5 simulations from the current-climate
318 were compared with those from the future-climate (under RCP8.5) to examine the influence
319 of increasing atmospheric greenhouse gas concentrations on regional scale TC characteristics
320 in the SH basins. The major findings of this work are summarised as follows.

321 • Compared to observations, CMIP5 models can realistically simulate regional TC
322 numbers and tracks reasonably well in the SH.

323 • TC track density is projected to decrease (~1–3 per decade) by the late twenty-first
324 century for coastal communities situated in the South Indian Ocean and Western
325 Australia. This was attributed to a significant decrease in TC numbers west of 130°E
326 (~18–42%; R1–R4) due to changes in environmental parameters such as reduced
327 relative humidity, relative vorticity and convergence.

- TC track density change over eastern Australia and the Coral Sea was found to be fairly minor (within ±1 TC per decade). Notably, poleward of 20°S on the eastern Australian coast, there was significant agreement between models of a small increase in track density (~1 per twenty years). This could be potentially due to an increase in the number of Coral Sea storms tracking westward (R6-West), increased lifetime of R5-East storms, or change in mean trajectory of R6-West storms.

- Over the South Pacific (R7), a decrease in TC track density was found (~1 per decade). This was attributed to a significant decrease in TC numbers (~ 15%), consistent with increased environmental vertical wind shear, and to a lesser extent, reduced low-level cyclonic vorticity and convergence.

- Projected changes in the mean lifetime of TC tracks in each region were also examined but no indication of any major change (> 1 day) between current- and future-climate simulations were established.

Overall, the projections of annual TC numbers given by this study are consistent with fine resolution (60 km) model experiments performed by Murakami et al. (2012) as they also showed a more confident reduction in TC numbers over the South Indian Ocean than the South Pacific (as per their Fig. 4). Using slightly coarser resolution model experiments, Rathmann et al. (2014) also showed similar results, emphasising that the significant decrease of TCs in the South Indian Ocean under RCP8.5 was consistent with more frequent early twentieth century (1900–1930) TCs. Similar to the present study, Sugi et al. (2014) attributed a less favourable large-scale environment to the widespread reduction of TC numbers in the South Indian Ocean. Our result of no major changes in TC track lifetimes was consistent with the results of Knutson et al. (2010) but in contrast to Rathmann et al. (2014) who projected TC lifetimes in the SP basin (i.e. in our R5–R7 regions) to decrease by 19%.

Future areas of scientific interest suggested by this study include: (1) the extent at which projected changes are modulated by ENSO, (2) quantitative assessment of the drivers of eastward and westward tracks in the regions R3–R6 with respect to natural modes such as monsoonal waves and ENSO, and (3) further investigation into the causes of a slight increase in TC activity poleward of 20°S on the eastern Australian coast.

Acknowledgements

Thanks to Hamish Ramsay and Paul Gregory for some useful comments to improve the paper. This work is supported through funding from the Earth Systems and Climate Change Hub of the Australian Government's National Environmental Science Programme (NESP). Samuel Bell is supported by an Australian Government Research Training Program (RTP) Stipend and RTP Fee-Offset Scholarship through Federation University Australia.

373 # Appendices

374 ## A. Robustness of multi-model ensembles

375 We test the robustness of the 12-M ensemble results as it may be argued that some key
376 assumptions may be violated on the following grounds.

377 (1) Model independence: presence of same family members in the ensemble.

378 (2) Model biases: models simulating TCs where they are not observed in the real world
379 (e.g. eastern South Pacific).

380 (3) Model reliability: ensuring models correctly simulate SH TC formation and track
381 climatology patterns.

382 (4) Sensitivity: exclusion of short lived TCs (<48-hrs) in the analysis.

383 We first address point (4) by repeating the 12-M analysis of Section 3a with short
384 lived (<48-hr) TCs included. It is found out of the 84 trials (12 models with 7 regions each)
385 there are only two models that indicate changes of sign from a reduction in TC numbers to an
386 increase (BCC-CSM1.1m changed from a 1% decrease to 4% increase in R2; while CNRM-
387 CM5 changed from a 17% decrease to a 2% increase in R3). Similarly, two other regions
388 changed sign from an increase in TC numbers to a decrease in two other models. Overall,
389 there is no change in the 95% significance of the sign tests for each region. Confidence
390 intervals of percentage change in TCs are also similar as the previous analysis (not shown).

391 To address points (1) - (3), we assess each model subject to the following criteria.

392 i. Detected model TCs should be within ±50% of observed climatology [0° – 225°E]

ii. Less than 5% of a model's TCs should form in the eastern South Pacific (between [230° – 300°E])[5]

iii. Spatial density correlations between model TC tracks and observed climatology should be above 0.85.

iv. Cluster analysis should produce similar clusters to the observed climatology (as in Fig. 2a).

In order to properly address these concerns (i. – iv.), a decision was made to create a new ensemble that only contains the models that best meet the above criteria. Knutti et al. (2013) derived a 'family tree' of CMIP5 models, documenting their similarities and highlighting how code sharing between institutions is behind some interdependency. Here, only one model from each family (e.g., Table A1) are allowed to be part of the new ensemble, to ensure independence is retained. Results for each model (Fig. A1; Table A1; Table A2) show that the models ACCESS1.0, CCSM4, MIROC5, BCC-CSM1.1M and CSIRO-MK3.6 meet all four criteria, and are therefore first choice members of the new ensemble. The B-tier includes ACCESS1.3 and HadGEM2-ES but as they share common characteristics with ACCESS1.0, these are not included in the ensemble. The three GFDL models all have similar errors from the criteria assessed, with GFDL-ESM2m managing the best score of "C". However, given that the emphasis of this ensemble is on track related performance, errant steering in the South Pacific makes this model unsatisfactory to include. Therefore, only the five A-tier models are used to form the 5-model ensemble (5-M).

[5] Some models produce TCs where they are not observed, particularly in the South Atlantic and eastern South Pacific [east of 135°W]. Storms forming in the eastern South Pacific are more of an issue here as they are nearby to where real TCs are observed to form, creating doubt around the correct simulation of nearby large-scale conditions necessary for TC formation. Therefore, this assessment criteria is put in place to potentially exclude models from the ensemble if more than 5% of a model's TCs form between [130°W and 60°W].

B. OWZ Detection and tracking

The OWZ detection system consists of six parameters (Table B1): minimum thresholds of OWZ at the 850- and 500 hPa levels, relative humidity (RH) at the 950- and 700 hPa levels, specific humidity (SpH) at the 950 hPa level and a maximum threshold of vertical wind shear (VWS) between 850- and 200 hPa. The OWZ variable is a low deformation vorticity parameter used to identify regions favourable for TC formation at the centre of a semi-closed circulation (i.e. a 'marsupial pouch'; Dunkerton et al. 2009), within the lower- to mid-troposphere. More precisely, it is the product of absolute vorticity and the Okubo-Weiss parameter (Okubo 1970; Weiss 1991) normalised by the vertical components of relative vorticity squared such that:

$$OWZ = sgn(f) \times (\zeta + f) \times \max\left[\frac{\zeta^2 - (E^2 + F^2)}{\zeta^2}, 0\right] \quad (1)$$

where f is the Coriolis parameter, $\zeta = \frac{\partial v}{\partial x} - \frac{\partial u}{\partial y}$ the vertical component of relative vorticity, $E = \frac{\partial u}{\partial x} - \frac{\partial v}{\partial y}$ the stretching deformation, and $F = \frac{\partial v}{\partial x} + \frac{\partial u}{\partial y}$ the shearing deformation.

The OWZ detection and tracking scheme is concisely summarized in five dot points below, with further detail accessible in other studies (Tory et al. 2013a; Bell et al. 2018).

a. Each 1º × 1º grid point is assessed based on the initial threshold values of each OWZ-Detector parameter every 12-hrs.
b. When at least two neighbouring grid points satisfy the initial thresholds of each OWZ-Detector parameter, these points are considered to represent a single circulation at that point in time.
c. The circulations from step (b) are linked through time by estimating their position in relation to the circulation's expected position based on an averaged 4º × 4º steering wind at 700 hPa.

d. Tracks are terminated when no circulation match is found in the next two time-steps within a generous (~350 km) latitude dependent radius.

e. The core thresholds are then applied to each storm track, and if they are satisfied for 48-hrs, a TC is declared.

References

Bell SB, Chand SS, Tory KJ, Turville C (2018) Statistical assessment of the OWZ tropical cyclone tracking scheme in ERA-Interim. *J. Climate*, **31**, 2217–2232

Brown JR, Moise AF, Colman RA (2012) The South Pacific Convergence Zone in CMIP5 simulations of historical and future climate. *Climate Dyn.,* doi: 10.1007/s00382-012-1591-x.

Bi D, Dix M, Marsland S et al (2012) The ACCESS Coupled Model: Description, Control Climate and Evaluation. *Aust. Meteor. Oceanog. J*., CMIP5 Special Issue, 63, 41-646

Camargo SJ (2013) Global and regional aspects of tropical cyclone activity in the CMIP5 models. *J. Climate*, **26**, 9880–9902

Camargo SJ, Robertson AW, Gaffney SJ, Smith P, Ghil M (2007) Cluster analysis of typhoon tracks. Part I: General properties. *J. Climate*, **20**, 3635-3653.

Chand SS, Walsh KJE (2009) Tropical cyclone activity in the Fiji region: Spatial patterns and relationship to large-scale circulation. *J. Climate*, **22**, 3877–3893.

Chand SS, Tory KJ, Ye H, Walsh KJE (2017) Projected increase in El Niño-driven tropical cyclone frequency in the Pacific. *Nature Climate Change*. **7**, 123–127, doi:10.1038/nclimate3181

Christensen JH, Krishna Kumar K, Aldrian E et al (2013) Climate phenomena and their relevance for future regional climate change. In: Stocker TF, and Co-authors, eds. *Climate Change 2013: The Physical Science Basis. Contribution of Working Group I to the Fifth Assessment Report of the Intergovernmental Panel on Climate Change* (IPCC AR5). Cambridge, UK and New York, NY: Cambridge University Press.

478 Colbert AJ, Soden BJ, Kirtman BP (2015) The impact of natural and anthropogenic climate
479 change on western North Pacific tropical cyclone tracks. *J. Climate*, **28**, 1806–1823

480 Collier MA, Jeffrey SJ, Rotstayn LD et al (2011) The CSIRO-Mk3.6.0 Atmosphere-Ocean
481 GCM: participation in CMIP5 and data publication. In: 19th International Congress on
482 Modelling and Simulation, Perth, Australia, 12–16 December 2011
483 http://mssanz.org.au/modsim2011

484 CSIRO and Bureau of Meteorology (2015) Climate Change in Australia (CCiA). Information
485 for Australia's Natural Resource Management Regions. Technical Report, *CSIRO and Bureau*
486 *of Meteorology*, Australia

487 Daloz AS, Camargo SJ, Kossin JP et al (2015) Cluster analysis of down-scaled and explicitly
488 simulated North Atlantic tropical cyclone tracks. *J. Climate*, **28**, 1333–1361,
489 doi:0.1175/JCLI-D-13-00646.1.

490 Donner LJ, Wyman BL, Hemler RS et al (2011) The dynamical core, physical
491 parameterizations, and basic simulation characteristics of the atmospheric component AM3 of
492 the GFDL global coupled model CM3. *J. Climate*, **24**, 3484–3519,
493 doi:10.1175/2011JCLI3955.1.

494 Dunkerton TJ, Montgomery MT, Wang Z (2009) Tropical cyclogenesis in a tropical wave
495 critical layer: Easterly waves. *Atmos. Chem. Phys*., **9**, 5587–5646.

496 Emanuel KA (2013) Downscaling CMIP5 climate models shows increased tropical cyclone
497 activity over the 21st century. *Proceedings of the National Academy of Sciences of the United*
498 *States of America*, **110**, 12,219–12,224, doi:10.1073/pnas.1301293110

499 Gaffney SJ (2004) Probabilistic curve-aligned clustering and prediction with regression
500 mixture models. Ph.D. thesis, University of California, Irvine, CA, 281 pp. [Available online
501 at http://www.ics.uci.edu/pub/sgaffney/outgoing/sgaffney_thesis.pdf.]

502 Gent PR, Danabasoglu G, Donner LJ et al (2011) The community climate system model
503 version 4. *J. Climate Special Collections*, **24,** 4973–4991

504 Gray WM (1975) Tropical cyclone genesis. *Dept. of Atmos. Sci.,* Paper No.234, Colorado
505 State University, Fort Collins, CO.

506 Grose MR, Brown JN, Narsey S, Brown JR, Murphy BF, Langlais C, Gupta AS, Moise AF,
507 Irving DB (2014) Assessment of the CMIP5 global climate model simulations of the western
508 tropical Pacific climate system and comparison to CMIP3. *Int. J. Climatol.,* **34**, 3382–3399.
509 doi:10.1002/joc.3916

510 Horn M, Walsh KJ, Zhao M et al (2014) Tracking scheme dependence of simulated tropical
511 cyclone response to idealized climate simulations. *J. Climate*, **27**, 9197–9213,
512 doi:10.1175/JCLI-D-14-00200.1

513 Jones CD, Hughes JK, Bellouin N et al (2011) The HadGEM2-ES implementation of CMIP5
514 centennial simulations. *Geosci. Model Dev.,* **4**, 543–570

515 Kossin JP, Emanuel KA, Vecchi GA (2014) The poleward migration of the location of
516 tropical cyclone maximum intensity. *Nature*, **509**, 349–352, doi:10.1038/nature13278

517 Kossin JP, Emanuel KA, Camargo SJ (2016) Past and Projected Changes in Western North
518 Pacific Tropical Cyclone Exposure. *J. Climate*, **29**, 5725–5739

519 Knapp KR, Kruk MC, Levinson DH, Diamond HJ, Neumann CJ (2010) The international
520 best track archieve for climate stewardship (IBTrACS) unifying tropical cyclone data. *Bull.*
521 *Am. Meteor. Soc*., **91**, 363–376

Knutson T, and Co-authors (2010). Tropical cyclones and climate change. *Nat Geosci.* **3**, 157–163

Knutti R, Masson D, Gettelman A (2013) Climate model genealogy: Generation CMIP5 and how we got there. *Geophys. Res. Lett.* **40**, 1194-1199

Moise A, Wilson L, Grose M et al (2015) Evaluation of CMIP3 and CMIP5 Models over the Australian Region to Inform Confidence in Projections. *Aust. Meteor. Oceanog. J.,* **65**, 19–53. DOI: 10.22499/2.6501.004

Murakami H, Mizuta R, Shindo E (2012) Future changes in tropical cyclone activity projected by multi-physics and multi-SST ensemble experiments using the 60-km-mesh MRI-AGCM. *Climate Dyn.,* **39**, 2569–2584

Nakamura J, Lall U, Kushnir Y, Camargo SJ (2009) Classifying North Atlantic Tropical Cyclone Tracks by Mass Moments. *J Climate.* **22**, 5481–5494

Nakamura J, Camargo SJ, Sobel AH et al (2017) Western North Pacific Tropical Cyclone Model Tracks in Present and Future Climates. *J. Geo. Phys. Research*, **122**, 1333–1361, doi:0.1175/JCLI-D-13-00646.1.

Okubo A (1970) Horizontal dispersion of floatable particles in the vicinity of velocity singularities such as convergences. *Deep-Sea Res.,* **17**, 445–454.

Park D-SR, Ho, C-H, Chan JCL, Ha K-J Kim H-S, Kim J, Kim J-H (2017) Asymmetric response of tropical cyclone activity to global warming over the North Atlantic and western North Pacific from CMIP5 model projections. *Scientific Reports*, **7**, 41354. doi:10.1038/srep41354.

Rathmann NM, Yang S, Kaas E (2014) Tropical cyclones in enhanced resolution CMIP5 experiments. *Climate Dyn*., **42**, 665–681

Riahi K, Rao S, Krey V, Cho C, Chirkov V, Fischer, G, Kindermann G, Nakicenovic N, Rafaj P (2011) RCP 8.5—A scenario of comparatively high greenhouse gas emissions. *Climatic Change,* **109**, 33-57, doi:10.1007/s10584-011-0149-y

Sanderson B, Knutti R, Caldwell P (2015) A Representative Democracy to Reduce Interdependency in a Multimodel Ensemble. *J. Climate*, **28**, 5171–5194

Shen Y, Sun Y, Camargo SJ, Zhong Z (2018) A Quantitative Method to Evaluate Tropical Cyclone Tracks in Climate Models. *J. Atmos. Ocean. Tech,* in press.

Sugi M, Yoshimura J (2012) Decreasing trend of tropical cyclone frequency in 228-year high-resolution AGCM simulations. *Geophys. Res. Lett*., **39,** L19805. doi:10.1029/2012GL053360.

Sugi M, Murakami H, Yoshimura J (2014) Mechanism of the Indian Ocean Tropical Cyclone Frequency Changes due to Global Warming. In: Mohanty U.C., Mohapatra M., Singh O.P., Bandyopadhyay B.K., Rathore L.S. (eds) Monitoring and Prediction of Tropical Cyclones in the Indian Ocean and Climate Change. Springer, Dordrecht. 40–49. doi:978-94-007-7720-0_4

Ramsay HA, Camargo SJ, Kim D. (2012) Cluster analysis of tropical cyclone tracks in the Southern Hemisphere. *Climate Dyn.,* **39**, 897–917, doi:10.1007/s00382-011-1225-8.

Taylor KE, Stouffer RJ, Meehl GA (2012) An overview of CMIP5 and the experiment design. Bull. Am. Meteor. Soc. **93**, 485–498

Tory KJ, Frank WM (2010) Tropical cyclone formation. Chapter 2: Global Perspectives on Tropical Cyclones, edited by: Chan J, Kepert JD, *World Scientific,* Second Edition

Tory KJ, Dare RA, Davidson NE, McBride JL, Chand SS (2013a) The importance of low-deformation vorticity in tropical cyclone formation. *Atmos. Chem. Phys*. **13**, 2115–2132

567 Tory KJ, Chand SS, Dare RA, McBride JL (2013b) The development and assessment of a
568 model-, grid- and basin independent tropical cyclone detection scheme. *J. Climate,* **26,** 5493–
569 5507

570 Tory KJ, Chand SS, McBride JL, Ye H, Dare RA (2013c) Projected changes in late 21st
571 century tropical cyclone frequency in thirteen coupled climate models from the coupled
572 model intercomparison project phase 5. *J Climate,* **26**, 9946–9959

573 Tory KJ, Dare RA (2015) Sea surface temperature thresholds for tropical cyclone formation. J
574 Climate, **28**, 8171–8183

575 Tory KJ, Ye H (2018) Projected Changes of Tropical Cyclone Formation Regions in the
576 Southern Hemisphere. In: 33rd Conference on Hurricanes and Tropical Meteorology, 16 – 20
577 April 2018. American Meteorological Society, Ponte Vedra, FL

578 Voldoire A, Sanchez-Gomez E, Salas y Mélia D et al (2012) The CNRM-CM5.1 global
579 climate model: description and basic evaluation. *Climate Dyn.,* **40**, 2091-2121

580 Walsh KJE, Katzfey JJ, (2000) The Impact of Climate Change on the Poleward Movement of
581 Tropical Cyclone–Like Vortices in a Regional Climate Model. *J. Climate,* **13**, 1116–1132

582 Walsh KJE, Fiorino M, Landsea CW, McInnes KL (2007) Objectively determined resolution-
583 dependent threshold criteria for the detection of tropical cyclones in climate models and
584 reanalyses. *J. Climate*, **20**, 2307–2314.

585 Walsh KJE, McBride JL, Klotzbach PJ, Balachandran S, Camargo SJ, Holland G, Knutson
586 TR, Kossin JP, Lee TC, Sobel A, Sugi M (2016) Tropical cyclones and climate change.
587 *WIREs Clim Change*. **7**, 65–89, doi:10.1002/WCC.371

588 Wang C, Wu L (2015) Influence of future tropical cyclone track changes on their basin-wide
589 intensity over the western North Pacific: Downscaled CMIP5 projections. *Adv. Atmos. Sci.*
590 **32**, 613–623

591 Watanabe M, Suzuki T, O'ishi R et al (2010) Improved climate simulation by MIROC5:
592 Mean states, variability, and climate sensitivity. *J. Climate*, **23**, 6312–6335,
593 doi:10.1175/2010JCLI3679.1.

594 Weiss J (1991) The dynamics of enstrophy transfer in two-dimensional hydrodynamics. *Phys.*
595 *D*, **48**, 273–294.

596 Wu T, Song L, Weiping L et al (2014) An overview of BCC climate system model
597 development and application for climate change studies. *J. Meteor. Res.,* **28,** 34–56,
598 doi:10.1007/s13351-014-3041-7.

599

Figure

FIGURES

`

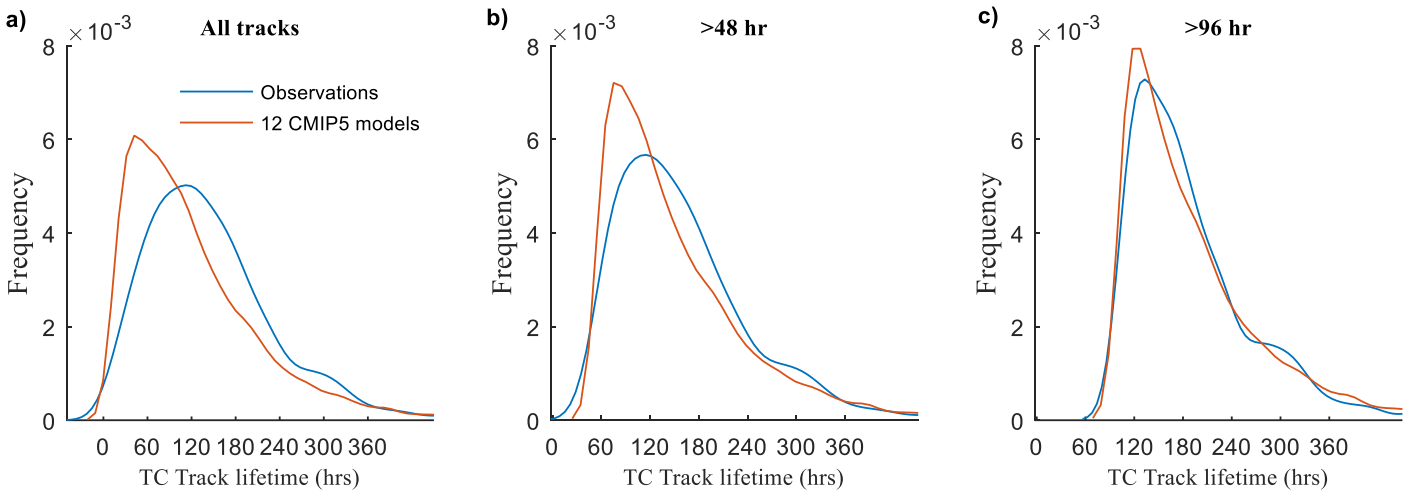

Fig. 1 Kernel density estimates of the distribution of TC track lifetimes for the observations (blue) and 12 CMIP5 models (orange). (a) all tracks, (b) only tracks that are of at least 48-hr lifetime, and (c) at least 96-hr lifetime.

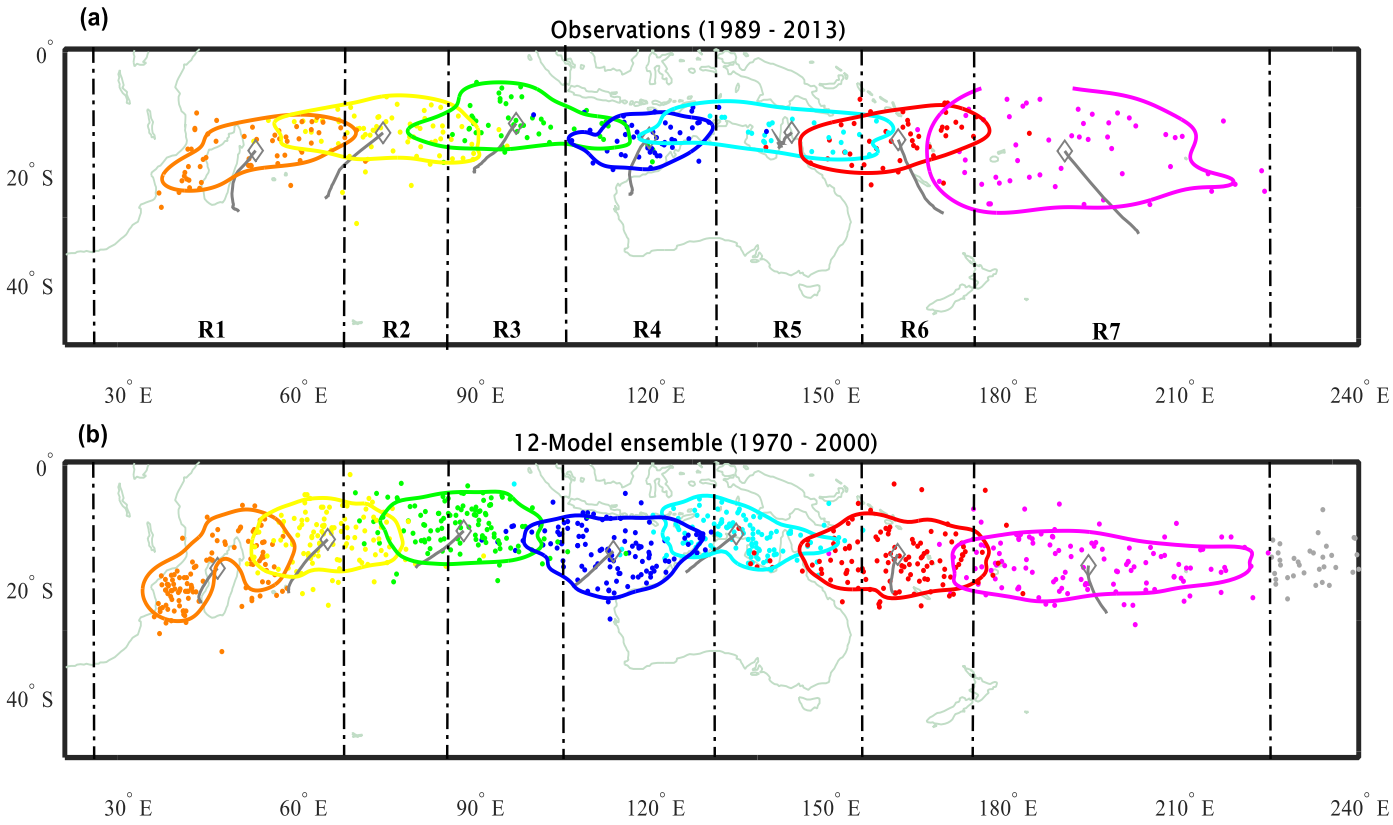

Fig. 2 Kernel density contours enclosing 75% of the TC genesis locations in each cluster. Up to 120 TC genesis locations are randomly selected from each cluster and displayed on the figure. Mean track trajectory and genesis (grey) for each cluster appear in the centre of the contours. Meridians define the seven genesis study regions (R1-R7) (black dash-dot lines).

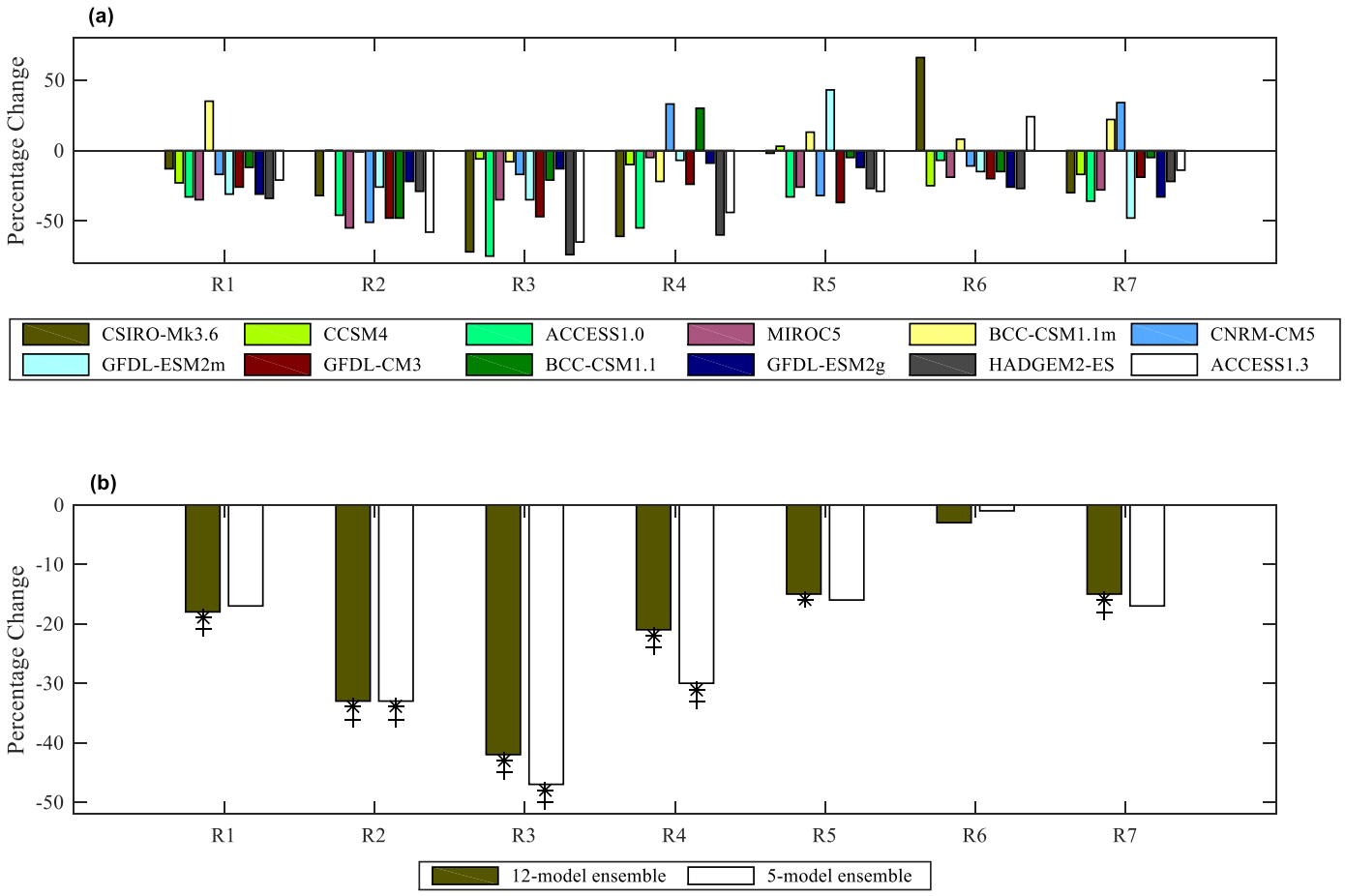

Fig. 3 (a) Percentage change in mean TC numbers in the CMIP5 models between the current climate simulation (1970-2000) and future climate projection (2070-2100). (b) As in (a) but for the 12-model and 5-model ensembles. Mean changes that are significant at 95% are indicated by an asterisk (*) while changes that have a 95% significant sign agreement of ensemble members are indicated by a plus (+) symbol.

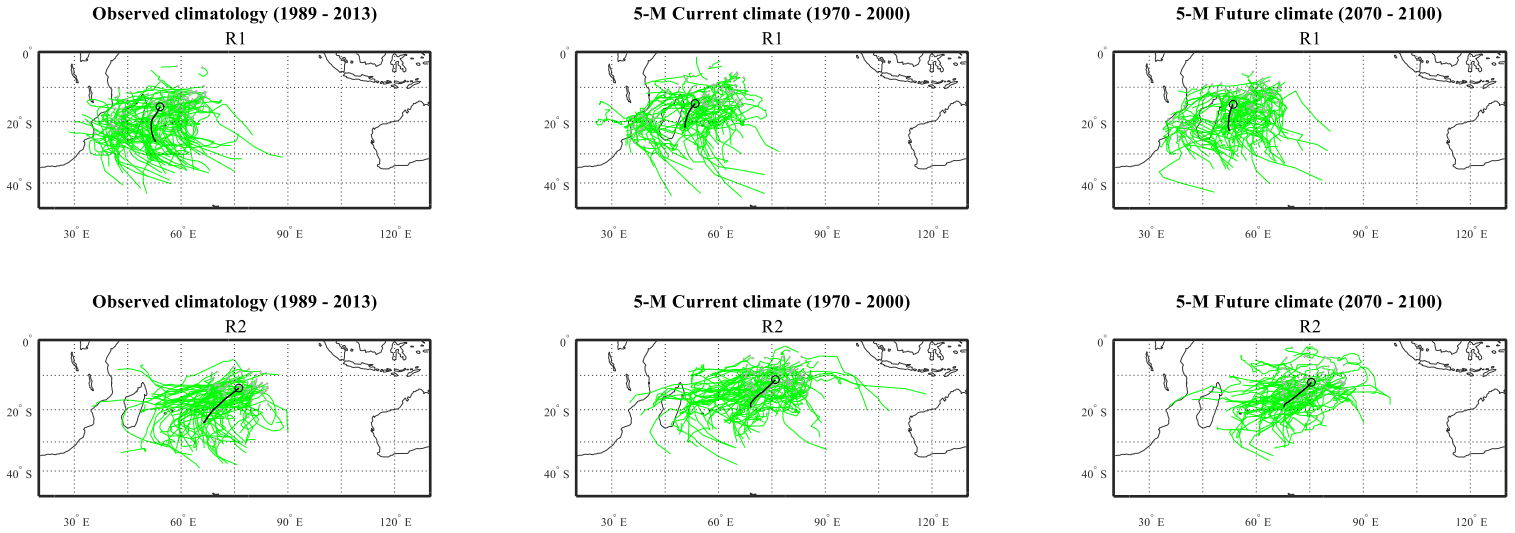

Fig. 4 Mean trajectories (to a mean plus two standard deviations in length, μ + 2σ) and individual TC tracks (random sample of up to 100) of observed and model tracks for the single cluster regions R1 and R2.

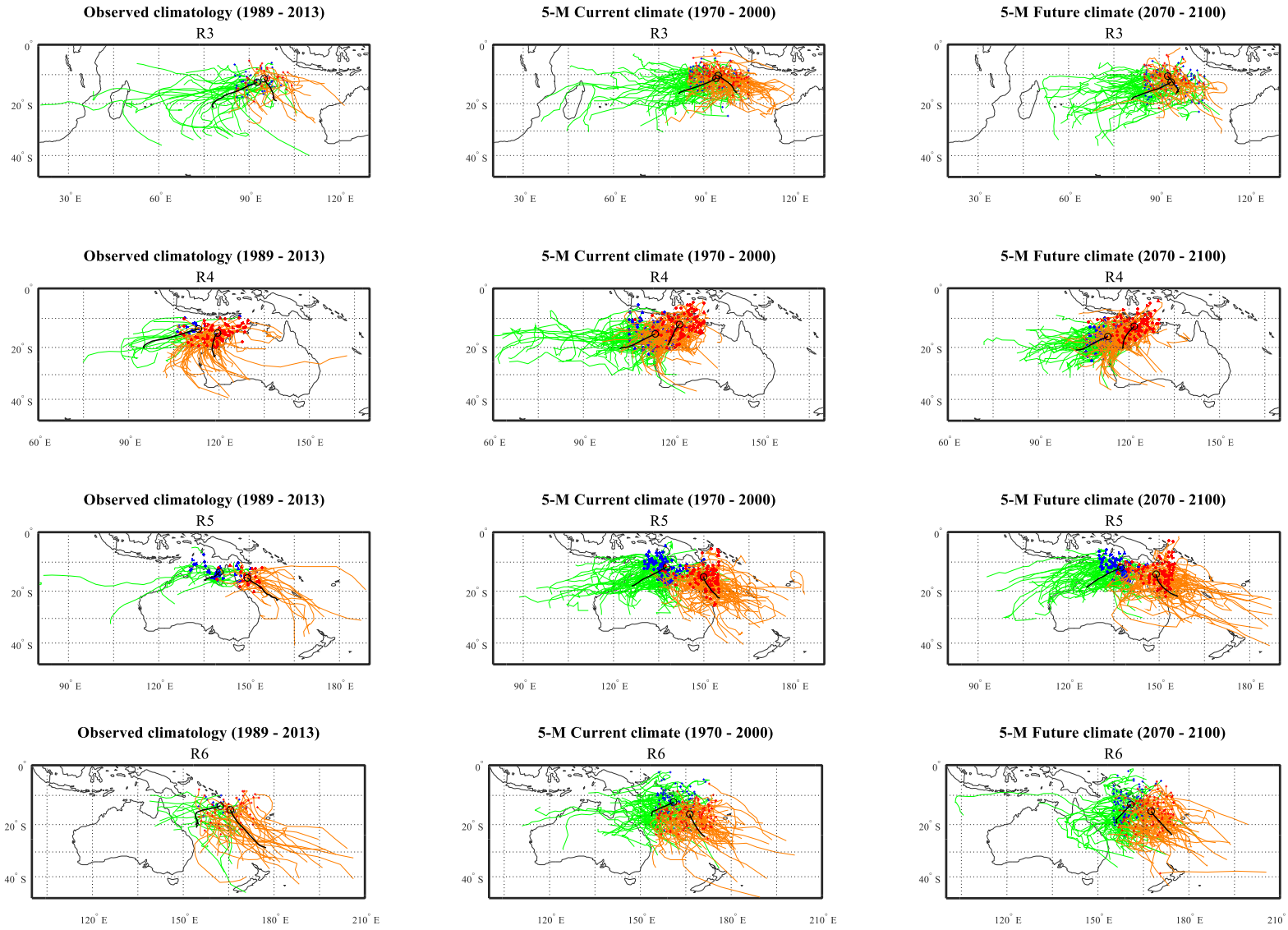

Fig. 5 As in Fig. 4, but for the 2-cluster regions (R3–R6). Note tracks in Region-3 are manually split into “west” and “east” tracks (see Footnote 4).

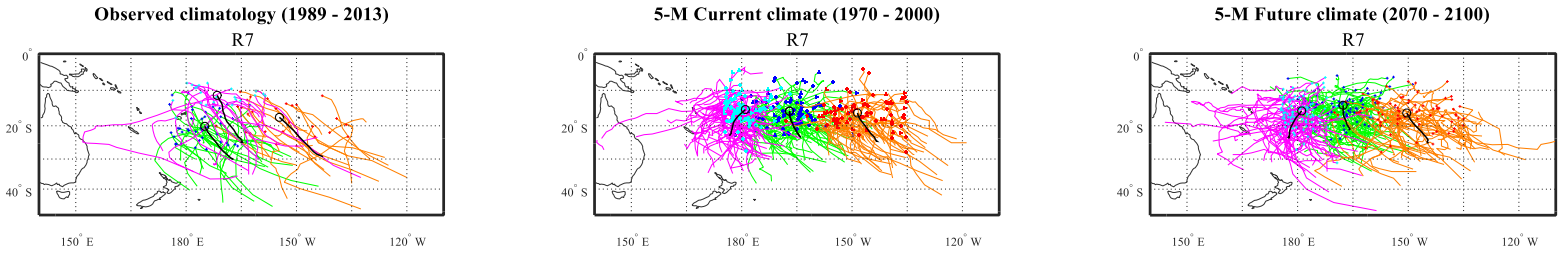

Fig. 6 As in Fig. 4, but for the 3-cluster region (R7).

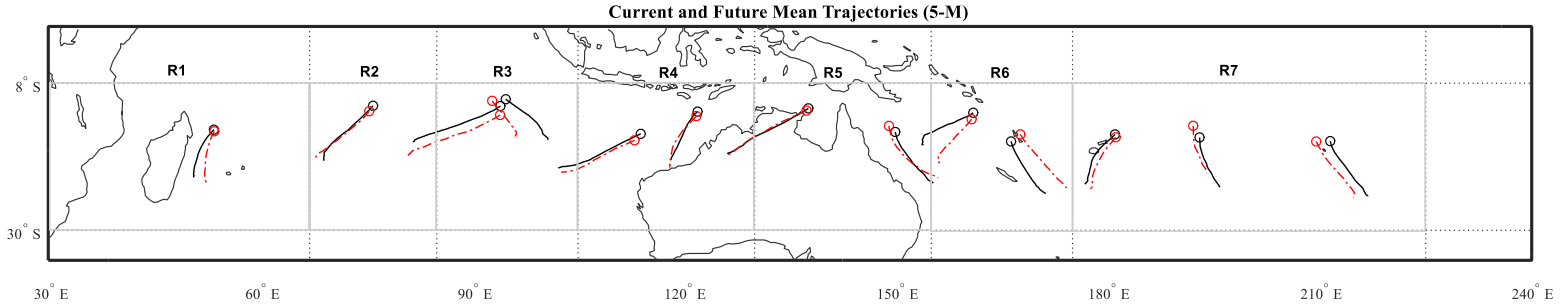

Fig. 7 Mean trajectories for the current (black) and future (red) climate 5-M ensemble simulations (as in Figs. 4,5,6).

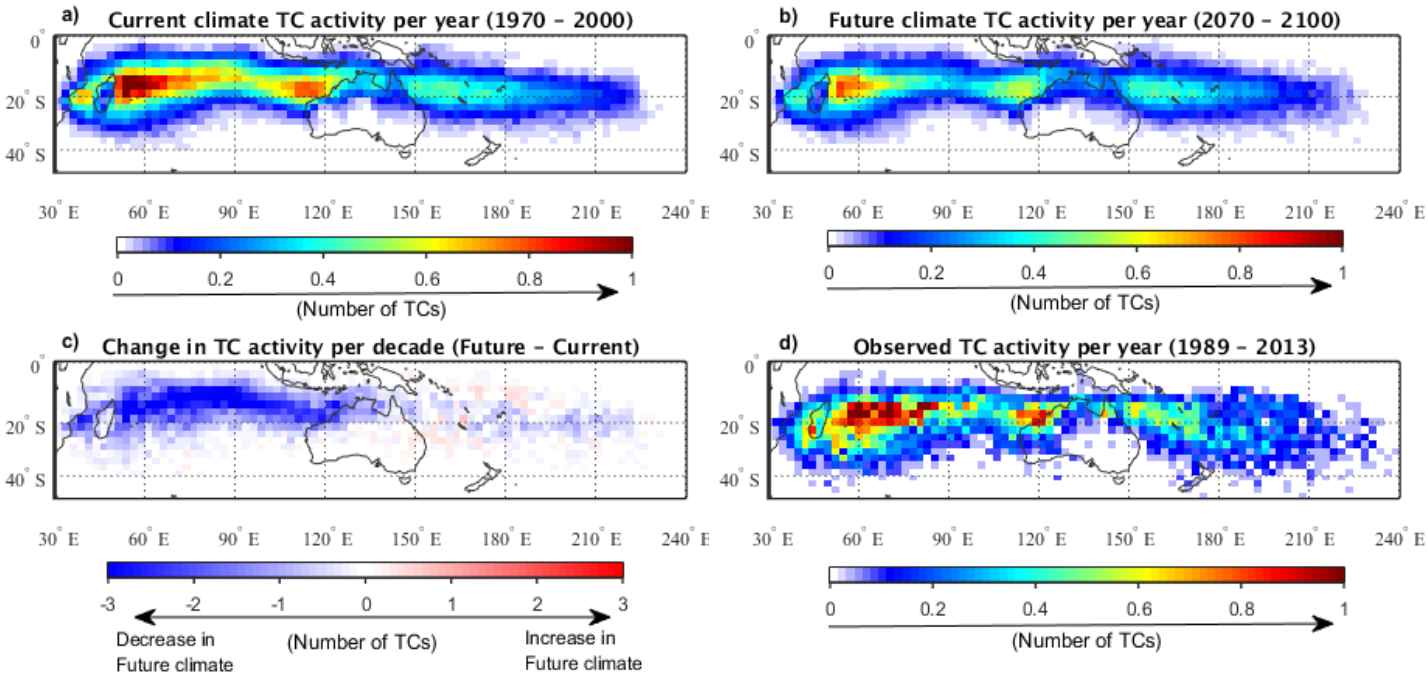

Fig. 8 TC activity (a measure of the number of unique TCs either entering or forming within a 2.5° x 2.5° grid-box) for the current- and future-climate 12-M simulations (a,b), projected change in TC activity between these simulations (c) and (d) TC activity observed in the IBTrACS database.

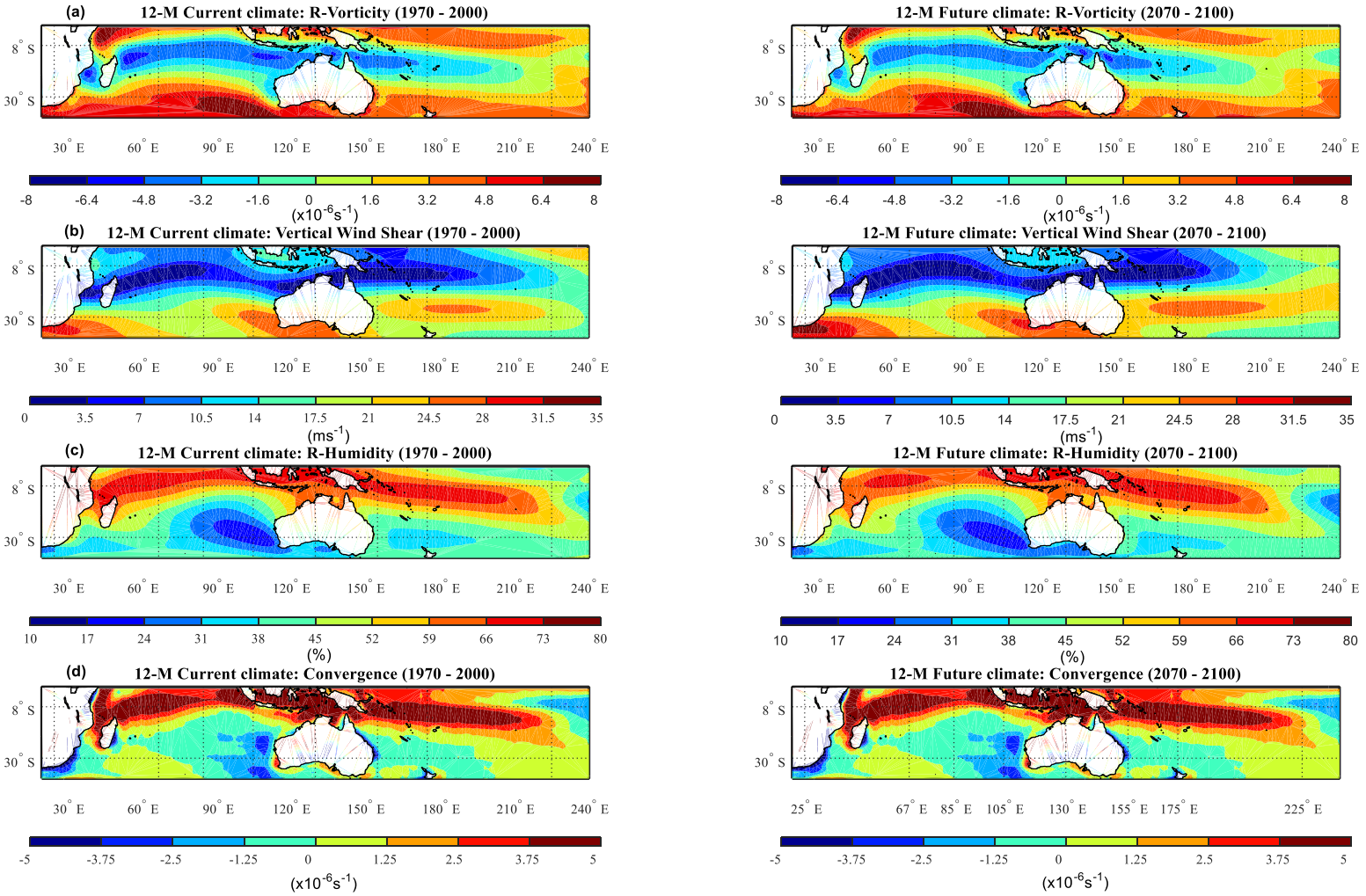

Fig. 9 Mean kernel density smoothed contours of large-scale TC genesis parameters for the current- and future-climate during the summer months (December-February). For (a) Relative vorticity at 850-hPa where blue (red) shading represents enhanced (suppressed) vorticity in the future climate, (b) environmental vertical wind shear between 250-hPa and 800-hPa where blue (red) shading represents increased (decreased) shear in the future climate, (c) Relative humidity at 700-hPa where red (blue) shading represents increased (decreased) relative humidity, and (d) Low-level convergence where red (blue) shading represents increased (decreased) convergence activity.

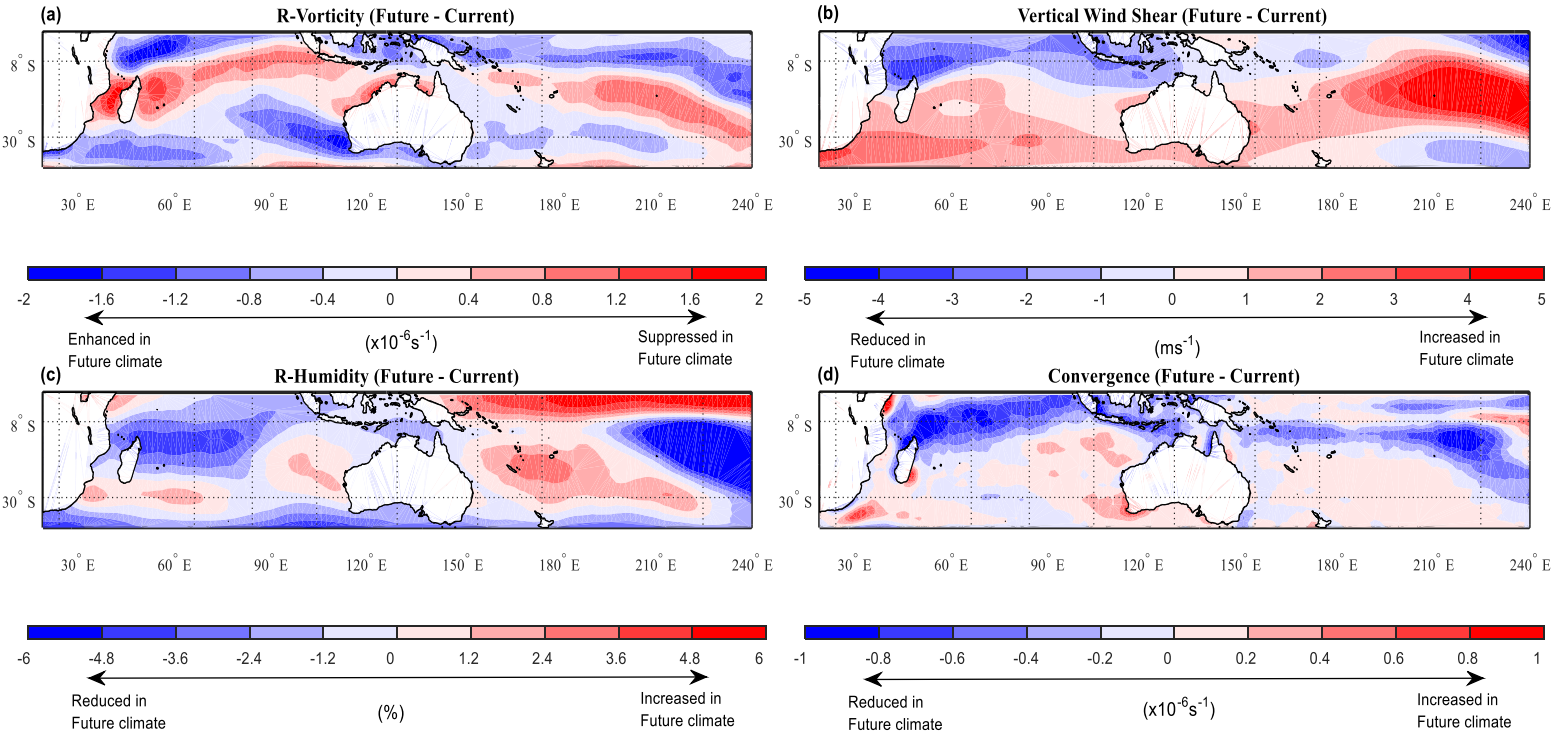

Fig. 10 Difference in the kernel densities of large-scale TC genesis parameters between the future-climate (FC) and current-climate (CC) 12-M ensembles during the summer months (December-February). (a) Relative vorticity at 850-hPa (R-Vorticity), (b) Environmental vertical wind shear between 250-hPa and 800-hPa, (c) Relative humidity at 700-hPa (R-Humidity), and (d) Low-level convergence (850-hPa).

Supplementary Figures (Appendix A)

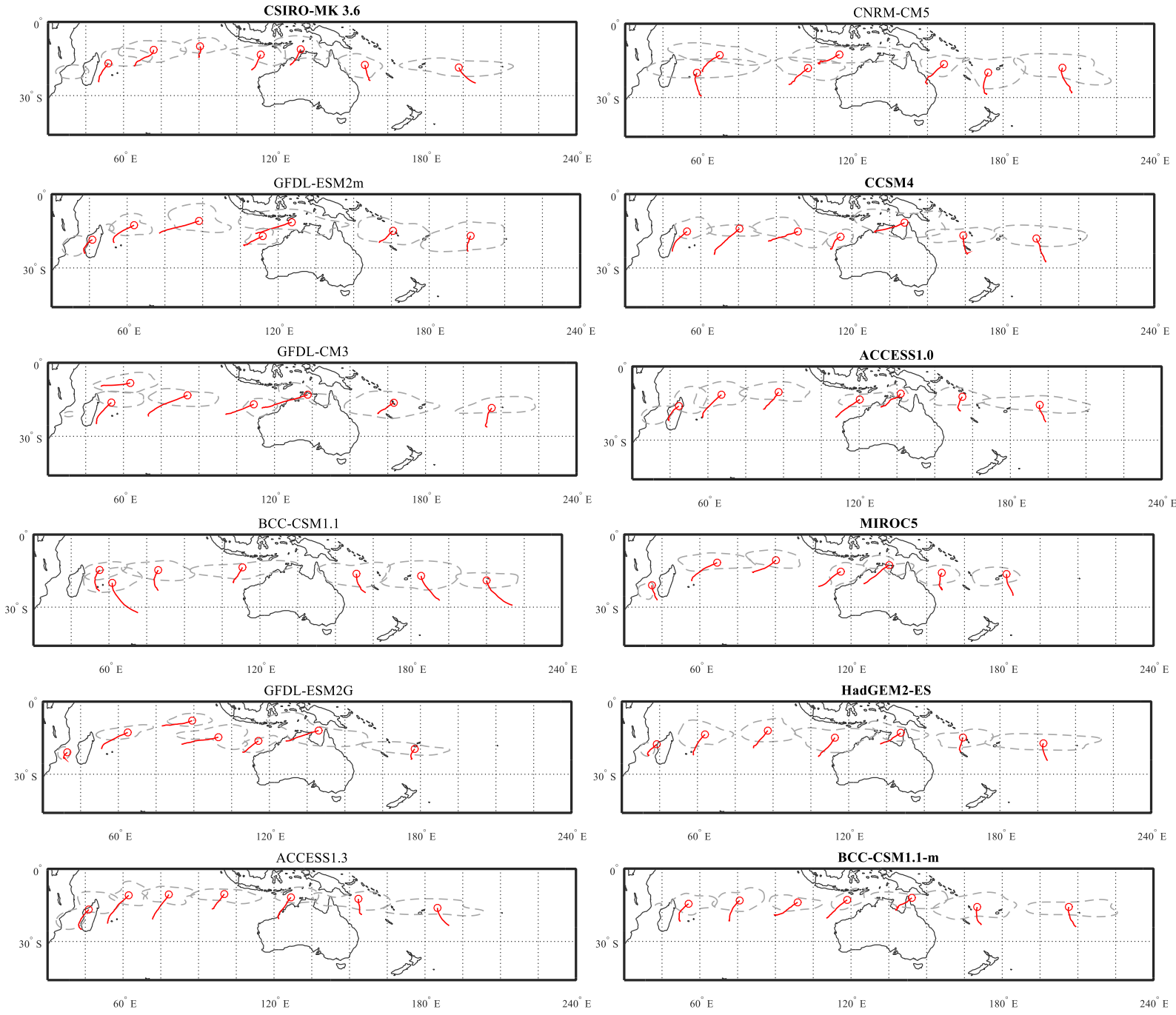

Fig. A1: 7-cluster solution for each CMIP5 model in the current climate (1970 – 2000). Mean TC trajectory and genesis (red line and circle) of a cluster with a kernel density contours enclosing 50% of the genesis points in that cluster (grey dashed). Models in bold indicates similar cluster orientations as the observations.

TABLES

Table 1: The twelve CMIP5 models used in this study. Number of TC detections (>2 day lifetime) between 0°E and 135°W in the Southern Hemisphere for the current-climate (1970–2000) and future-climate (2070–2100) under RCP8.5. All models listed form the 12-M ensemble, those in bold form the 5-M ensemble.

Model	**Horizontal Resolution**	**TC Detections**		**Reference**
		Current	**Future**	
GFDL-ESM2M	2.5°	848	643	Donner et al. 2011
GFDL-CM3	2.5°	812	568	Donner et al. 2011
GFDL-ESM2G	2.5°	784	624	Donner et al. 2011
ACCESS1.0	1.9°	967	599	Bi et al. 2012
ACCESS1.3	1.9°	1078	771	Bi et al. 2012
HadGEM2-ES	1.9°	1150	710	Jones et al. 2011
BCC-CSM1.1	2.8°	588	507	Wu et al. 2014
BCC-CSM1.1M	2.8°	649	703	Wu et al. 2014
CSIRO-Mk3.6	1.9°	980	670	Collier et al. 2011
CNRM-CM5	1.4°	322	301	Voldoire et al. 2012
CCSM4	1.2°	509	439	Gent et al. 2011
MIROC5	1.4°	1038	755	Watanabe et al. 2010

Table 2: Mean annual TC numbers (and proportion of that region's numbers) in the seven regions observed in IBTrACS (1989–2013), and from model ensemble current climate simulation (1970–2000), and future climate projection (2070–2100) under RCP8.5. Difference between future and current model TC numbers (Change). Number of models in agreement on the sign of change in TC occurrences (Sign). Sign and 95% Confidence Interval (CI) values in bold indicate significance at the 95% level. An asterisk (*) indicates one model in that region had the same number of TC occurrences in both current and future climate simulations.

12-model ensemble						95% CI	
Region	Observed	Current	Future	Change	Sign	Lower	Upper
R1	4.2 (20.4%)	6.2 (23.5%)	5.1 (24.3%)	**-18%**	**11/12**	**-0.30**	**-0.06**
R2	3.2 (15.4%)	3.5 (13.3%)	2.4 (11.3%)	**-33%**	**11/11***	**-0.45**	**-0.21**
R3	2.7 (12.9%)	3.1 (11.6%)	1.8 (8.5%)	**-42%**	**12/12**	**-0.58**	**-0.26**
R4	3.3 (16%)	4.2 (15.8%)	3.3 (15.8%)	**-21%**	**10/12**	**-0.39**	**-0.03**
R5	1.9 (9.3%)	2.5 (9.7%)	2.2 (10.4%)	-15%	9/12	**-0.29**	**-0.01**
R6	2.5 (12%)	2.9 (11%)	2.8 (13.5%)	-3%	9/12	-0.19	0.13
R7	2.9 (13.9%)	3.9 (15%)	3.4 (16.1%)	**-15%**	**10/12**	**-0.29**	**-0.01**
5-model ensemble						95% CI	
Region	Observed	Current	Future	Change	Sign	Lower	Upper
R1	4.2 (20.4%)	5.9 (22%)	4.9 (23.8%)	-17%	4/5	-0.43	0.08
R2	3.2 (15.4%)	3.7 (13.8%)	2.5 (12.2%)	**-33%**	**4/4***	**-0.55**	**-0.10**
R3	2.7 (12.9%)	3.4 (12.7%)	1.8 (8.8%)	**-47%**	**5/5**	**-0.77**	**-0.17**
R4	3.3 (16%)	4.6 (17.2%)	3.2 (15.7%)	**-30%**	**5/5**	**-0.53**	**-0.07**
R5	1.9 (9.3%)	3.1 (11.6%)	2.6 (12.7%)	-16%	3/5	-0.34	0.01
R6	2.5 (12%)	2.8 (10.6%)	2.8 (13.7%)	-1%	3/5	-0.34	0.31
R7	2.9 (13.9%)	3.2 (12%)	2.7 (13.1%)	-17%	4/5	-0.38	0.04

Table 3: Mean annual TC numbers in each cluster further split into "westward" and "eastward" trajectories by cluster analysis or otherwise. Information appears as: *Mean annual TC numbers (Frequency percentage for that region).* Westward and eastward splits are implied by 2-cluster solutions (see Fig. 4,5,6), except for Region-3* and Region-7 (see Footnote 4). Projected changes are between the future and current 5-M mean annual TC numbers, those that are consistent with 12-M results (increase or decrease) are in bold.

Region	Observed (1989-2013)	Current (1970-2000)	Future (2070-2100)	Projected Change
R3				
R3-West*	1.72 (62%)	2.31 (68%)	1.41 (79%)	**-39%**
R3-East*	1.04 (38%)	1.09 (32%)	0.38 (21%)	**-65%**
R4				
R4-West	0.68 (18%)	2.20 (48%)	1.65 (51%)	**-25%**
R4-East	3.00 (82%)	2.41 (52%)	1.57 (49%)	**-35%**
R5				
R5-West	1.56 (60%)	1.77 (57%)	1.19 (46%)	**-33%**
R5-East	1.04 (40%)	1.32 (43%)	1.40 (54%)	+6%
R6				
R6-West	0.76 (29%)	1.08 (38%)	1.26 (45%)	**+16%**
R6-East	1.84 (71%)	1.77 (62%)	1.54 (55%)	**-13%**
R7				
R7-West	-	1.09 (34%)	0.92 (34%)	**-16%**
R7-East1	1.51 (42%)	1.24 (39%)	0.99 (38%)	**-20%**
R7-East2	1.16 (32%)	0.89 (28%)	0.78 (28%)	**-12%**

Table 4: Mean TC track lifetimes in each region and sub-region as observed in IBTrACS and as detected in models by the 5-M ensemble. †R5-West observed tracks are often terminated at or soon after landfall, causing a discrepancy with model tracks.

Region	Observed (1989-2013)	Current (1970-2000)	Future (2070-2100)
R1			
	7.3 days	6.6 days	6.4 days
R2			
	7.5 days	7.6 days	6.7 days
R3			
R3-West*	8.7 days	7.5 days	6.8 days
R3-East*	5.1 days	5.6 days	5.1 days
R4			
R4-West	6.3 days	5.7 days	5.1 days
R4-East	5.3 days	6 days	6 days
R5			
R5-West	4.8† days	8.3 days	8.2 days
R5-East	6.9 days	6.7 days	7.6 days
R6			
R6-West	7.2 days	7.4 days	7.1 days
R6-East	5.8 days	5.4 days	5.2 days
R7			
R7-West	-	5.6 days	5.6 days
R7-East1	3.4 days	5.4 days	5.7 days
R7-East2	3.8 days	4.7 days	4.9 days

Supplementary Tables (Appendix A)

Table A1: Criteria assessment of each CMIP5 model. Values in bold indicate that a model has failed to meet a certain criterion. Scores are given based on how well they meet the four criteria with "A" the best performing and "D" the worst. Members chosen for the 5-model ensemble have their scores underlined in the final column. See Table A2 for more information.

Model	C1	C2	C3	C4		Score
Family-1						
GFDL-ESM2M	848	0.03	0.87	**N**	E4;E5	C
GFDL-CM3	812	**0.05**	0.90	**N**	E1;E5	D
GFDL-ESM2G	784	0.01	**0.80**	**N**	E1;E4;E5	D
Family-2						
ACCESS1.0	967	0.00	0.86	Y		A
ACCESS1.3	1078	0.00	0.87	**N**	E4	B
HadGEM2-ES	**1150**	0.02	0.93	Y		B
Family-3						
BCC-CSM1.1	588	**0.09**	**0.82**	**N**	E2;E3	D
BCC-CSM1.1M	649	0.04	0.91	Y		A
(No family)						
CSIRO-Mk3.6	980	0.00	0.85	Y		A
CNRM-CM5	**322**	**0.05**	0.86	**N**	E3	D
CCSM4	509	0.00	0.93	Y		A
MIROC5	1038	0.00	0.90	Y		A

Table A2: Information for Table A1. "*x*" represents a value in Table A1 for each model assessed.

Criteria	
C1	+-50% observed TC numbers, (364 <*x*<1092)
C2	% TCs in Eastern South Pacific, (*x*<0.05)
C3	Spatial correlation with observed, (*x*>0.85)
C4	Cluster result with observed, [Y=Similar, N=Not similar]
Cluster Error Codes	
E1	Low Latitude (<10*S) cluster in South Indian Ocean
E2	Too many clusters in South Pacific Ocean
E3	No cluster north of Australia
E4	Too many clusters in South Indian Ocean
E5	Westward mean trajectory in South Pacific Ocean